Construction and Building Materials 263 (2020) 120558

Contents lists available at ScienceDirect

Construction and Building Materials

journal homepage: www.elsevier.com/locate/conbuildmat

Self-cleaning and air purification performance of Portland cement paste with low dosages of nanodispersed TiO_2 coatings

Zixiao Wang [a,b,*], Florent Gauvin [b], Pan Feng [a,c], H.J.H. Brouwers [b], Qingliang Yu [b]

[a] Jiangsu Key Laboratory of Construction Materials, School of Materials Science and Engineering, Southeast University, Nanjing 211189, China
[b] Department of the Built Environment, Eindhoven University of Technology, P.O. Box 513, 5600 MB Eindhoven, the Netherlands
[c] State Key Laboratory of High Performance Civil Engineering Materials, Nanjing 210008, China

HIGHLIGHTS

- The stable nanodispersed anatase TiO_2 particles are synthesized in hydrosol form.
- The TiO_2 hydrosol-based coating presents a much better self-cleaning performance than that of P25 suspension.
- The TiO_2 hydrosol-based coating shows excellent air purification properties.

ARTICLE INFO

Article history:
Received 13 October 2019
Received in revised form 19 July 2020
Accepted 13 August 2020
Available online 6 September 2020

Keywords:
TiO_2 hydrosol
Synthetic temperature
Air purification performance
Self-cleaning coatings
Portland cementitious materials

ABSTRACT

The strong agglomeration potential and poor re-dispersibility of nano TiO_2 particles in powder form seriously affect the depollution and self-cleaning performances. The nano TiO_2 particles in hydrosol form can be stably dispersed in aqueous solution, but the synthetic temperature influences the crystal pattern, stability, and hydrodynamic diameter of nano TiO_2 particles. In this study, a stable and nano dispersed anatase TiO_2 hydrosol is synthesized by hydrolysis of titanium isopropoxide, and the effects of synthetic temperature on physicochemical properties and stability of TiO_2 hydrosol are discussed. The photocatalytic and self-cleaning performances of synthetic TiO_2 hydrosol coating are characterized by the colour change rate of Rhodamine B and NO_x conversion UV irradiation. Compared with a commercial nano TiO_2 powder (Degussa P-25), the TiO_2 hydrosol coating with very low dosages shows better photocatalytic and self-cleaning performances under the same experimental conditions.

1. Introduction

Cementitious materials in buildings are directly and continuously exposed to various atmospheric pollutants and micro-organisms under different weather conditions. Colour, the main index of aesthetic properties of buildings, must give a pleasant appearance that should give the public an adequate perception of the quality with the low necessity of maintenance. The leading cause of colour change on the surface of cementitious materials is the reduction in initial solar reflectivity, mainly from atmospheric aerosol pollutants such as nitrogen oxides, carbon-based materials (for example, soot), and volatile organic compounds [1,2]. Nano TiO_2-based coatings have been studied to improve the air purification and the self-cleaning property of cement-based materials [3-10]. The nano TiO_2 powders (for example, Degussa P25) [6,11-13] have been used as concrete coatings to enhance the photocatalytic activity. However, due to the inherent agglomeration and poor re-dispersity of nano TiO_2 powders in the aqueous system [14], the air-purifying and self-cleaning of coatings made of TiO_2 nanopowders are impacted obviously. Thus, a relatively high dosage of nano TiO_2 powders is often used to obtain good depollution performance, which leads to lower transparency of coatings and economic issues.

According to the previous studies [14-20], the photoactivity of nano TiO_2 particles is significantly associated with the crystal pattern, crystalline particle size, and size distribution of nanoparticles in aqueous synthetic nano TiO_2, which are demonstrated by the different synthesis processes of nano TiO_2. There are many methods to synthesize nano TiO_2, but the sol–gel process is widely used because of its advantages including such as high purity, excellent uniformity, the controllable microstructure of product, easier, low temperature, and low cost in processing. The heat treatment of calcination in the sol–gel process is necessary to transform

* Corresponding author at: Jiangsu Key Laboratory of Construction Materials, School of Materials Science and Engineering, Southeast University, Nanjing 211189, China.
E-mail address: z.wang3@tue.nl (Z. Wang).

https://doi.org/10.1016/j.conbuildmat.2020.120558
0950-0618/

amorphous TiO_2 to crystalline when the route is the commonly used polymeric route [14,17,20,21]. In this polymeric route, the solvent is usually alcohol, and the hydrolysis of titanium alkoxide precursors is carefully controlled by using a limited amount of water. However, the solvent is water in the second route [21,22], in which process the produced TiO_2 nanoparticles in hydrosol is crystalline without the step of calcination. Acids are used as peptizators to produce a TiO_2 hydrosol containing nanoparticles with a hydrodynamic diameter in the range of 15 nm to 100 nm. The crystalline TiO_2 nanoparticles are predominantly anatase with brookite and rutile, depending on the used acids [21,23,24].

Moreover, TiO_2 hydrosol [20-22,25-32] has a much larger specific surface area and is much more transparent than conventional TiO_2 nanopowder catalysts, which demonstrated better performance for the photocatalytic degradation of pollutants. As the photodegrading reactions between pollutants and coatings occur on the surface of TiO_2 particles [33], the excellent dispersity of nano TiO_2 particles in a liquid is critical that influences self-cleaning and photocatalytic performances of coatings. The stability of the TiO_2 hydrosol is another factor that needs to be considered in the synthetic process. For large-scale production of TiO_2-based coatings (for example, roller coating), the long-term stability of TiO_2 hydrosol is required to achieve acceptable repeatability. However, very few studies are available on the effects of synthesis temperature on the stability of TiO_2 nanoparticle dispersion in water.

This study investigates the influences of synthetic temperature in the so-gel process on the dispersion stability of produced TiO_2 hydrosol in water. In a second step, the self-cleaning and air purification performances of TiO_2 hydrosol-based coatings are tested by applying on the hardened cement paste's surface at the age of 7 days.

2. Materials and experimental

2.1. Materials

Titanium tetra-isopropoxide (TTIP, 97.0%) is purchased from Sigma-Aldrich. Glacial acetic acid (99.6%), and absolute ethanol (99.9%), are purchased from VWR Chemicals. Deionized water (18.2 MΩ.cm) is used throughout the development process of TiO_2 hydrosol. The nano TiO_2 powder (P25) is purchased from Evonik Industries AG company. The P25 powder contains about 75 wt% of anatase and 25 wt% of rutile, with the primary crystalline particle size of 10 to 50 nm and the specific BET surface area of 50 ± 15 m^2/g [3,34].

The selected method in this study to produce anatase TiO_2 hydrosols is adapted from studies from Yang et al. [35] and Alphonse et al. [21], but the different synthesis temperatures are applied. The synthesis is as follows: TTIP is dissolved in absolute ethanol with the TTIP/ethanol molar ratio of 2.44, the solutions are stirred for 30 min at different temperatures (50 °C and 40 °C). The obtained solution is added drop by drop at the speed of 0.01 mL/s into a mixture containing acetic acid and deionized water with a molar ratio of 0.175. After that, the suspension is continuously stirred for 48 h at 50 °C or 40 °C by magnetic stirrers and then left to settle for at least 72 h at a room temperature of 20 °C and relative humidity of 60%.

CEM I 52.5 R cement and tap water are used to prepare cement paste samples with the water to cement ratio of 0.4. Two different sizes of samples are prepared for different characterization tests. The paste samples in the size of 40 × 40 × 40 mm^3 are prepared for testing the surface self-cleaning performance and reflectance property after coating the prepared TiO_2. The paste samples in the size of 100 × 200 × 5 mm^3 are prepared for testing the NO_x degradation performance. After one day curing at the ambient environment, the paste samples are demoulded and cured in curing chamber (95% R. H. and 20 °C) till further tests. The top surfaces of cement paste samples are polished by SiC sandpapers to obtain relatively smooth surfaces with the roughness in the range of 10 μm to 14 μm. The synthetic TiO_2 hydrosol and P25 water suspension, which have the same mass content of TiO_2 particles, are coated on the surface of hardened cement paste samples. One cement paste sample is prepared for each coating dosage in the same test.

2.2. Methods

2.2.1. Characterization

The phase composition of the dried TiO_2 powder sample is investigated by comparing X-ray diffraction (XRD) pattern (Bruker D4 PHASER, Philips, The Netherlands) with a Co tube (40 kV, 40 mA). A typical run used in this test is made with a step size of 0.02°/min and a dwell time of 0.5 s. The crystallite size (D_c), also named the primary particle size [36], of the anatase phase is estimated from the Scherer's equation [24].

$$D_c = k\lambda/\beta cos\theta \quad (1)$$

where K = 0.89, λ = 0.154 nm, β is the full-width height maximum in radians, and θ is the Bragg's angle.

The particle size distribution and zeta potential of TiO_2 hydrosol are tested by the Zetasizer NanoSeries (Malvern Panalytical) at 25 °C. In these tests, the initial hydrosol is diluted 100 times in distilled water. The TiO_2 hydrosol samples are tested three times by Zetasizer Nano Series using a Dynamic Light scattering process. The Zetasizer Nano Series calculated the zeta potential by determining the electrophoretic mobility and then applying the Herny equation.

The UV–VIS absorbance spectra of TiO_2 hydrosol and P25 suspension samples are measured by the UV–VIS-NIR spectrophotometer (Perkin Elmer Lambda 750) tested range is 250 nm to 800 nm, 1 nm per second. According to the Beer-Lambert law, the sample content should be lower than 0.01 M, and the absorbance should be set below 1.0, in this study, the P25 suspension sample is diluted down to 0.02% and the TiO_2 hydrosol sample is diluted down to 1.0% by distilled water.

To measure the specific surface area and crystal phase pattern of the TiO_2 hydrosol sample, the powder sample is prepared by drying the initial TiO_2 hydrosol in the oven at 105 °C for 24 h. The specific surface area of dried TiO_2 hydrosol is measured by The Brunauer, Emmett, and Teller (BET) method. The pore size distribution from the adsorption isotherm is evaluated by the Barrett-Joyner-Halenda (BJH) interpretation. Nitrogen sorption isotherm experiments are carried out at 77 K temperature by a nitrogen adsorption/desorption device of type TriStar II 3020.

2.2.2. Self-cleaning performance of coated cement paste

The self-cleaning performance of the TiO_2 coated cement paste is evaluated by colorimetric analysis of the degradation of the organic dye Rhodamine B (RB) [37]. The coated weights of TiO_2 particle in TiO_2 hydrosol coatings are 0.77 g/m^2, 1.54 g/m^2, and 3.08 g/m^2. The cement paste samples without TiO_2 coating and coated P25 water suspension with the coating dosage of 1.54 g/m^2 are tested as the reference groups. After coating the TiO_2, the paste samples are dried in a dark box for 12 h under an ambient temperature of 20 °C. After pre-coated with TiO_2 hydrosol or P25 suspension, the top surfaces of cubic cement paste samples are stained by painting 600 uL of 0.1 mM RB aqueous solution. Then the cement paste samples are also dried in a dark box at 20 ℃ for 12 h. For each tested cement paste sample, nine points are considered for the colorimetric tests and each point is tested four times. The samples are exposed to a UV lamp (10 ± 0.05 W/m^2)

to simulate UV light in natural outdoor conditions, monitoring the discoloration of the RB on the surface of mortar.

The reflected colour measurements are taken directly on the surface of each point on each sample at different illumination with a spectrometer USB4000 Oceanoptics, which is optimized for the 380–780 nm wavelength range and analyzed mathematically to yield colorimetric quantities like xyz, RGB or L*a*b*. In this study, the percentage of discoloration (R_t) is expressed with the coordinate of the dominant colour of dye a*, a value of the CIE Lab colour space for RB [38-40], according to Eq. (2).

$$R_t(\%) = \frac{a_0^* - a_t^*}{a_0^*} \times 100 \tag{2}$$

Where, a_0^* the value of a* at time 0 before irradiation, a_t^* its value after t minutes irradiation.

2.2.3. Air purification performance of coated cement paste

The air purification experiments [6,7,11,41] of coated cement paste are carried out in a homemade reactor designed following the standard ISO 22197–1. The contents of TiO_2 particles in hydrosol and P25 suspension coatings are 1.54 g/m^2 and 3.08 g/m^2. The experimental setup, as shown in Fig. 1, consisted of a planar reactor cell, an UVA light source, a chemiluminescent NOx analyzer, and gas supply. The chief operating conditions of the system are as follows: the wavelength of UV light resource is 300 nm to 400 nm, the irradiance flux on the surface of flat cement paste samples is 10 ± 0.05 W/m^2, the pollutant source concentration is 1.0 ppm, the NO flow, and airflow are 0.06 L/min and 2.94 L/min, and the total gas flow is 3.0 L/min, the relative humidity in the reactor is 50 ± 1%. The amount of NO_x converted in the reactor is calculated following:

$$NO_X Conversion(\%) = \frac{[C_{NOX}]_{in} - [C_{NOX}]_{out}}{[C_{NOX}]_{in}} \times 100 \tag{3}$$

Where $[C_{NOx}]_{in}$ is the initial concentration [ppm], measured by taking the average value of the first 5 min of the experiment, before turning on the light. The outlet concentration $[C_{NOx}]_{out}$ is measured by taking the average value of the last 5 min of the irradiation period [ppm].

The amount of NO converted in the reactor is calculated following:

$$NOConversion(\%) = \frac{[C_{NO}]_{in} - [C_{NO}]_{out}}{[C_{NO}]_{in}} \times 100 \tag{4}$$

Where $[C_{NO}]_{in}$ is the initial concentration [ppm], measured by taking the average value of the first 5 min of the experiment, before turning on the light. The outlet concentration $[C_{NO}]_{out}$ is measured by taking the average value of the last 5 min of the irradiation period [ppm].

3. Results and discussions

3.1. Phase type of TiO_2 in hydrosol

The diffraction angle 2θ of (101) crystal plane of anatase TiO_2 crystal is 29.4°, the (004) crystal plane is 44.2° and the (200) (105) and (204) crystal planes are 56.4°, 63.5°, and 74.3°, respectively [42]. As can be seen in Fig. 2, the TiO_2 particles in hydrosol synthesized at 40 °C and 50 °C shows all the typical diffraction peaks of anatase, indicating the synthesized TiO_2 particles in hydrosol are pure anatase crystals. According to the calculations applying Eq. (1), the crystalline sizes of synthetic TiO_2 particles are 12 nm and 16 nm in hydrosol samples with processing temperatures of 40 °C and 50 °C, respectively. These results prove that the crystal pattern of TiO_2 particles in hydrosols is less impacted by the tested temperatures in synthesis processes, while the calculated crystal size of TiO_2 is decreased by 21.0% if the synthetic temperature reduces from 50 °C to 40 °C. Moreover, compared with the crystalline size of TiO_2 particles in P25 nanopowder (50 to 100 nm), the crystalline sizes of TiO_2 particles in synthetic hydrosols are much smaller. Generally, for nano photocatalysts, a smaller crystalline size significantly influences the photoactivity. In coatings, small particle size is expected to cause a larger surface area to volume ratio, leading to better dispersion and higher reactivity [43,44]. The dispersion of synthetic TiO_2 hydrosols will be discussed in the following section.

3.2. Dispersion stability of TiO_2 hydrosols

For physically stable nanosuspensions, a minimum zeta potential of ± 30 mV is required in an electrostatic stabilization, and a minimum of ± 20 mV is sufficient for steric stabilization [45-47]. The hydrodynamic diameters and Zeta potential values of synthetic TiO_2 hydrosol samples are shown in Table 1. The hydrodynamic diameters (D_H) of TiO_2 in hydrosol samples with the processing temperatures of 40 °C and 50 °C are 19 nm and 38 nm. The zeta potential of TiO_2 hydrosol synthesized at 40 °C and 50 °C are 43 mV and 39 mV, respectively. These results indicate that the synthesis temperature impacts the D_H of TiO_2 in

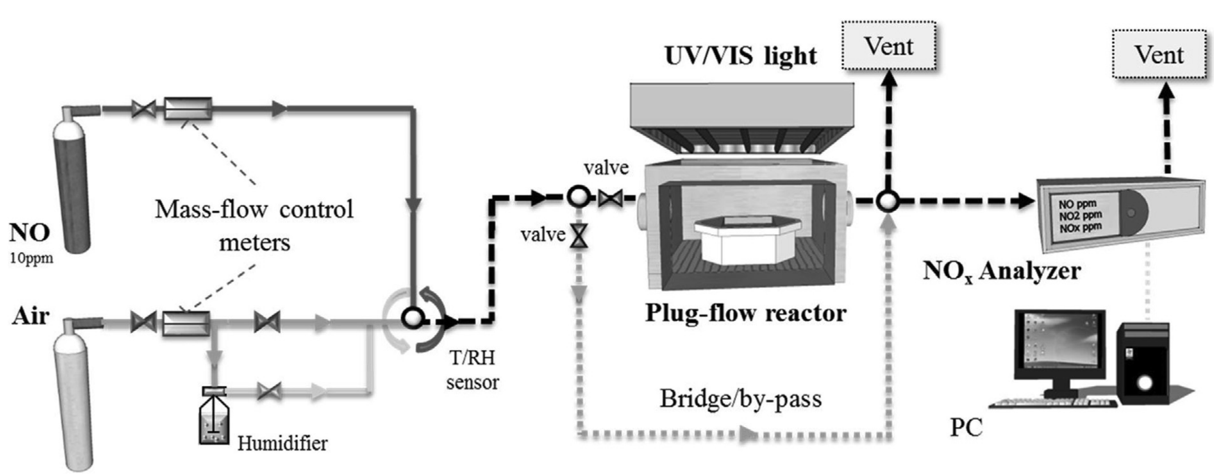

Fig. 1. The scheme of air purification experimental setup [6]

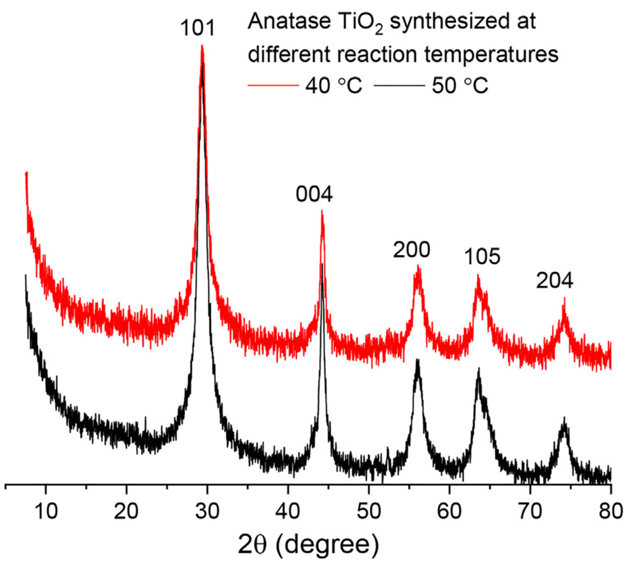

Fig. 2. XRD pattern of TiO_2 hydrosols dried at 105 °C.

hydrosol samples, while the zeta potential of TiO_2 hydrosols is less influenced. Compared with the primary crystalline sizes mentioned in Section 3.1, the D_H of particles in TiO_2 hydrosol sample synthetic at 50 °C increases to 2.4 times of the primary particles, indicating the primary particles may have agglomerated because of the van der Waals forces. While the D_H of particles in TiO_2 hydrosol sample synthetic at 40 °C increases to 1.6 times of the primary particles, demonstrating that the TiO_2 nanoparticles have relatively good dispersion and low agglomeration in this hydrosol form.

The polydispersity index (PI) is defined as the particle size distribution and its range of nanosuspensions. The physical stability of nanosuspensions can be evaluated by the PI value, indicating a nanosuspension with the smallest possible PI shows a long-time stability. A PI lower than 0.1 indicates a near-monodisperse particle distribution, a PI in the range of 0.1 to 0.25 shows a narrow size distribution of nanoparticles, and a PI larger than 0.5 means a very broad distribution of particle size [36,47,48]. As shown in Table 1, the PI values of the TiO_2 hydrosol synthesized at 40 °C and 50 °C are 0.11 and 0.14, respectively. Although the PI values in both TiO_2 hydrosol samples are larger than 0.1, it could be confirmed that the TiO_2 particles are closer to a near-monodisperse distribution in the hydrosol sample synthetic at 40 °C.

According to previous results [36], the mean particle size of P25 suspension ranges between 198 and 231 nm, with an average value of 221 ± 11 nm, and an average PI ranges 0.2 to 0.6. Compared with the primary particles with the size of 30 to 50 nm, the TiO_2 particles in P25 suspension are agglomerates or aggregates with much larger particle sizes, and poor disperse stability. Compared with P25 suspension, these results prove that the TiO_2 hydrosol synthesized at 40 °C obtains smaller primary crystalline size, smaller hydrodynamic diameter and better disperse stability. Thus, the following characterization tests are focused on the comparison between TiO_2 hydrosol synthesized at 40 °C and P25 suspension.

3.3. Optical analysis

The visual images and the UV–VIS absorbance spectra of TiO_2 hydrosol and P25 suspension with the mass content are shown in Fig. 3. As can be seen from Fig. 3(a), TiO_2 hydrosol is transparent, while the P25 suspension sample with the same mass content is pure white and non-transparent. The transparent TiO_2 hydrosol is another reliable evidence proving that the TiO_2 particles in hydrosol are tiny and dispersed stable. The main reason for the white of P25 suspension is that the particle sizes of TiO_2 aggregates in suspension are more significant than the wavelength of visible light, which reflects all wavelengths of visible light (400 to 800 nm) equally without wavelength selectivity. Moreover, as shown in Fig. 3(b), the absorbance of visible light in the range from 400 to 800 nm of P25 suspension is caused by the large aggregates of TiO_2 primary particles. The visual results confirm that the synthetic TiO_2 hydrosol presents good dispersion and better absorbance in the range of UV light.

3.4. BET specific surface area

The nitrogen isotherm plot of dried TiO_2 hydrosol is shown in Fig. 4 (a). The cumulative and differential pore size distribution plots of dried TiO_2 hydrosol are shown in Fig. 4 (b). In Fig. 4(a), the isotherm is a combination of type IV [49,50], which is associated with capillary condensation taking place in mesopores, and the limiting uptake over a range of high p/p0. The initial part of the Type IV isotherm, for example, $0 < p/p_0 < 0.1$ in Fig. 4(a), is attributed to monolayer-multilayer adsorption since it followed the same path as the corresponding part of a Type II isotherm obtained with the given adsorptive on the same surface area of the adsorbent in a non-porous form. At a relative pressure between 0.4 and 0.8, there is one hysteresis loop, which corresponded to the smaller pore fraction and indicated that the pore size distributions of dried TiO_2 are unimodal pore size distributions in the mesoporous region [51]. Hysteresis appearing in the multilayer range of physisorption isotherms is usually associated with capillary condensation in mesopore structures. The shape of the hysteresis loop is type H2 associated, which could be observed in the pores with narrow necks and more extensive bodies (often referred to as 'ink bottle' pores) [50]. It could be seen from Fig. 4(b) that the dried TiO_2 hydrosol shows unimodal pore size distributions of small mesopores (about 3 nm). Due to the finer intra-aggregated pore, small mesopores are formed between TiO_2 grains or primary particles (represented by the hysteresis loop in the p/p_0 range from 0.4 to 0.8).

Table 2 shows the BET specific surface area and pore parameters of dried TiO_2 hydrosol. Total pore volume is taken from the volume of nitrogen adsorbed at p/p0 = 0.985. The average pore diameter is estimated using the adsorption branch of the isotherm and the Barrett–Joyner–Halenda (BJH) formula. As shown in Table 2, the BET specific surface area of dried TiO_2 hydrosol is 244.8 m^2/g, which is about five times larger than that of P25 (about 50 m^2/g [3,34,52]). The absorption average pore width in dried hydrosol samples is 5.2 nm, indicating the mesopores have mainly existed among TiO_2 aggregates. The BET test results illustrate that the dried TiO_2 aggregates transformed from the hydrosol form contain

Table 1
Parameters of dispersion stability for synthetic TiO_2 hydrosols.

Synthesis temperatures	Hydrodynamic diameters± SD (d. nm)	Zeta potential(mV)	PI	Conductivity(mS/cm)
50 ℃	38 ± 16	39	0.14	0.12
40 ℃	19 ± 6	43	0.11	0.11

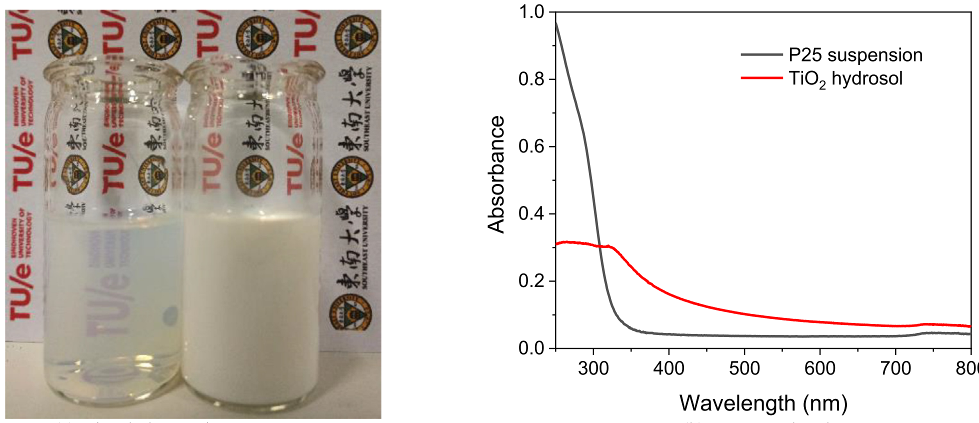

(a) Visual observation (b) UV-VIS absorbance spectra

Fig. 3. The visual observation and UV–VIS absorbance spectra of TiO_2 hydrosol and P25 suspension (The left image in (a) is TiO_2 hydrosol, the right image in (b) is P25 suspension with the same dosage of 1.54 wt%).

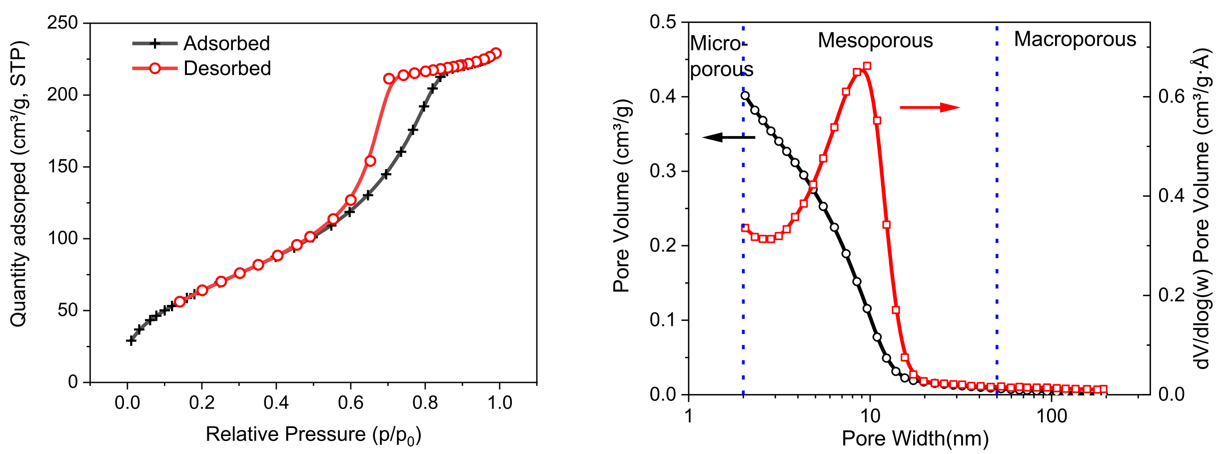

(a) Nitrogen isotherm plot (b) Pore size distribution

Fig. 4. The corresponding nitrogen isotherm plot and pore size distribution of dried TiO_2 hydrosol.

Table 2
BET specific surface area and pore parameters of dried TiO_2 hydrosol.

Hydrolysis temperature (°C)	BET specific surface area (m^2/g)	Pore volume (ml/g)	Pore size (nm)
40	244.8	0.35	5.2

lots of mesopores and a relatively larger specific surface area, which are necessary for a coating with high photoactivity. The self-cleaning and air purification properties of dried coatings should be evaluated when applying photocatalytic coatings on the cement-based materials. The photocatalytic self-cleaning and air purification performances of TiO_2 hydrosol-based coating on the surface of hardened cement paste will be discussed in Sections 3.5 and 3.6.

3.5. Self-cleaning performance

The uncoated hardened cement paste (HCP) sample and the HCP sample coated with the P25 suspension with the TiO_2 dosage of 1.54 g/m^2 are designed as the control samples in the self-cleaning tests. The colour change rate (R_t) for RB of coated cement paste samples at the age of 7 days is shown in Fig. 5. The R_t values of HCP samples coated with TiO_2 hydrosol with the dosages of 0.77 g/m^2, 1.54 g/m^2, and 3.08 g/m^2 after four hours irradiation are 79.9%, 90.1%, and 91.1%, respectively. The R_t values of HCP samples coated with TiO_2 hydrosol with the dosages of 0.77 g/m^2, 1.54 g/m^2, and 3.08 g/m^2 after 24 h irradiation are 85.9%, 91.7%,

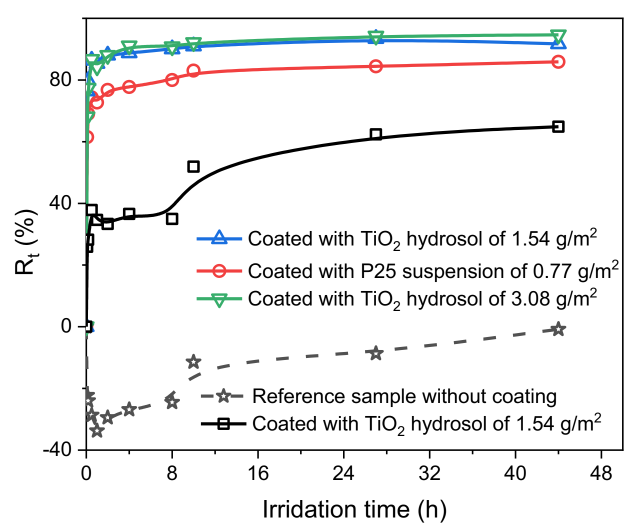

Fig. 5. Percentage of colour change for RB on the surface of cement paste samples coated with different coatings after seven days hydration.

and 94.7%, respectively. The colour change of the blank cement sample is around zero after 24 h irradiation, indicating the blank cement presents very poor self-cleaning performance. The R_t of cement paste coated by P25 with the dosage of 1.54 g/m^2 after 24 h irradiation is only 64.9%. Moreover, in the TiO_2 hydrosol coated HCP samples, the R_t trends stabilize after two hours irradiation, while it needs at least 6 h irradiation to obtain a stable R_t in the P25 coated HCP sample. These results suggest that the photocatalytic self-cleaning performance of HCP paste coated with 1.54 g/m^2 TiO_2 in the form of hydrosol is much better than that of the form of P25 suspension.

According to the test results in the previous sections, the well-dispersed TiO_2 nanoparticles in dried TiO_2 hydrosol coating contain lots of mesopores and obtain a large BET specific surface area, providing more reactive regions for the photochemical reactions between TiO_2 and RB molecules. As a result, the TiO_2 hydrosol coating shows excellent photoactivity in degrading the dried RB film on the surface of hardened cement paste.

3.6. Air purification performance

The air purification properties of the TiO_2 hydrosol coating and P25 suspension coating are evaluated by the conversion rates of NO and NO_x under UV irradiation. Fig. 6 shows the recorded degradation results of NO, NO_2, and NO_x of HPC panel samples coated with different dosages at the age of seven days. The calculated conversion rate of NO and NO_x are shown in Table 3.

As shown in Fig. 6, the NO and NO_x conversion rates of the TiO_2 hydrosol coating are barely influenced by the coated dosage of TiO_2 nanoparticles, but that of the P25 suspension coating is impacted obviously. The NO concentration reduced from 1 ppm to about 0.05 ppm in a few minutes in the tested panel coated by TiO_2 hydrosol with a coating dosage of 1.54 g/m^2. As to the panel sample coated by the TiO_2 hydrosol coating with the dosage of 3.08 g/m^2, the NO concentration decreases to about 0.1 ppm after a few minutes UV irradiation, and then continuously decreases to about 0.01 ppm after 120 min of UV irradiation. When coated with 1.54 g/m^2 of P25 suspension, the NO concentration reduces to about 0.05 ppm from 1 ppm. However, when the coated dosage of P25 suspension increases to 3.08 g/m^2, the NO concentration reduces to about 0.15 ppm from 1 ppm. The coated dosage of the P25 suspension hampers the NO degrading efficiency, indicating the reactive region of TiO_2 particles reduces with the increase of P25 suspension coating.

Table 3
The conversion rates of NO and NO_x of two coatings on the surface of HPC panel samples.

Coated dosage (g/m^2)	Coatings	NO conversion rate (%)	NO_x conversion rate (%)
1.54	TiO_2 hydrosol	97.4	93.9
1.54	P25 suspension	97.7	95.0
3.08	TiO_2 hydrosol	98.9	96.1
3.08	P25 suspension	87.9	86.0

As shown in Table 3, at a lower coated dosage of TiO_2 nanoparticles (1.54 g/m^2), both NO and NO_x conversion rates of two coatings are higher than 90%, and the NO and NO_x conversion rates of the TiO_2 hydrosol and the P25 suspension are very close. When the coated dosage of TiO_2 nanoparticles increases to 3.08 g/m^2, the NO and NO_x conversion rates of the TiO_2 hydrosol coating are 1.5% and 2.3% higher than that with the coated dosage of 1.54 g/m^2. However, with a higher coated dosage, the NO and NO_x conversion rates of P25 suspension coating are 10% and 9.5% lower than those with a coated dosage of 1.54 g/m^2.

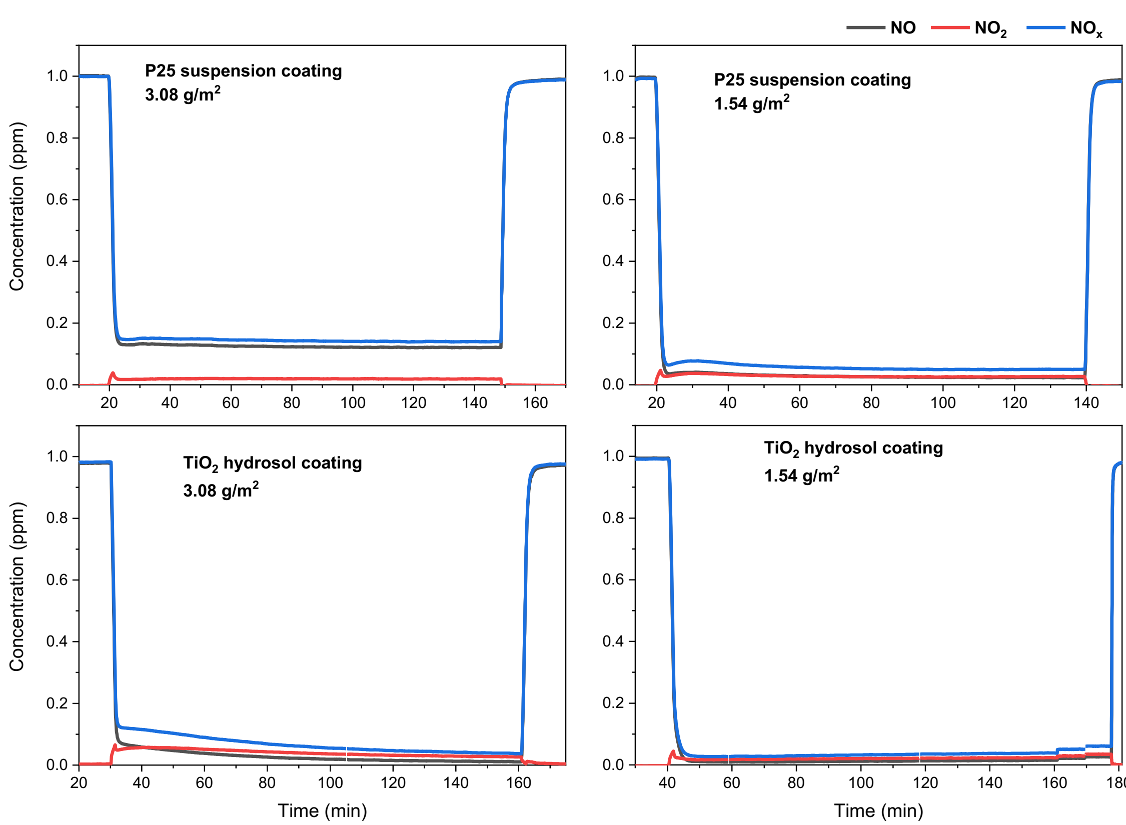

Fig. 6. NO, NO_2 and NO_x concentration graphs of cement panel samples coated with TiO_2 hydrosol and P25 suspension coatings.

Here, comparing the degradation of organic dye film and inorganic gas pollutants, it is easy to find out that the synthetic TiO_2 hydrosol can degrade both RB and NO with high efficiencies. However, the P25 suspension shows unsatisfied efficiency in degrading RB. The reason for this significant difference may be related to the attachment between two kinds of target molecules and coatings. The RB water solution on the surface of coated hardened cement paste samples, after the evaporation of water, the RB molecules are distributed on the surface of coatings. While, NO and air fill the whole reactor evenly during the air purification test. Due to the small primary crystalline size, nano-scale hydrodynamic diameter and good disperse stability, the TiO_2 particles can be well dispersed in the dried TiO_2 hydrosol coating on the surface of hardened cement paste samples without too much agglomeration. The excellent dispersion means that the TiO_2 particles in dried hydrosol coating can provide more reactive areas for photodegrading RB and NO molecules. As a result, the synthetic TiO_2 hydrosol coating can obtain excellent photocatalytic self-cleaning performance and good air purification performance.

4. Conclusions

In this work, the nano dispersed TiO_2 hydrosol is synthesized by an easy and low energy consumption method. The particle size and zeta potential are tested to evaluate the water disperse stability of TiO_2 nanoparticles in hydrosol form. The specific surface area and the pore size distribution of dried TiO_2 agglomerates from hydrosol form are measured by BET tests. The photocatalytic self-cleaning performance and air purification performance of TiO_2 hydrosol by coating on the surface of hardened cement paste (HCP) samples are compared with that of commercial P25 nano TiO_2 powder.

(1) The primary crystalline size and hydrodynamic diameters of TiO_2 particles in hydrosol are influenced by the peptizing temperature. Compared with the primary particles, the TiO_2 nanoparticles in hydrosol with the synthetic temperature of 40 ℃ shows good dispersion and low agglomeration. The TiO_2 particles resulted from the dried synthetic hydrosol are pure anatase with a large BET specific surface area.

(2) The TiO_2 hydrosol coatings with three different TiO_2 dosages present much better photocatalytic self-cleaning performance in degrading RB film on the surface of HCP samples. The degradation rate of RB increases with the coated dosage of TiO_2 particles in hydrosol coatings. Even with the lowest coated dosage (0.77 g/m^2), more than 85% of RB molecules are degraded by the TiO_2 hydrosol coatings after 24 h of UV irradiation, while only 64.9% of RB molecules are degraded by the P25 suspension coating with the coated dosage of 1.54 g/m^2.

(3) The TiO_2 hydrosol coatings with different coated dosages present excellent air purification performance with the conversion rates of NO and NO_x higher than 90%. Nevertheless, the higher the coated dosage of P25 suspension coating, the lower the conversion rates of NO and NO_x. With a lower coated dosage (1.54 g/m^2), the P25 suspension coating presents the same good NO and NO_x conversion ability with the TiO_2 hydrosol coating. While, with a higher coated dosage (3.08 g/m^2), the NO and NO_x conversion rates of the P25 suspension coating reduce by around 10% compared with the rates with a lower coated dosage; on the contrary, the NO and NO_x conversion rates of the TiO_2 hydrosol coating increase by about 2%.

(4) When applying the nano TiO_2-based coatings on cement-based materials, the high NO_x conversion rates not always mean the excellent degradation efficiencies of organic dye. Thus, evaluating the photocatalytic ability of coatings by degrading dried organic dyes is necessary for applying on cement-based materials.

CRediT authorship contribution statement

Zixiao Wang: Conceptualization, Methodology, Investigation, Data curation, Formal analysis, Validation, Writing - original draft. **Florent Gauvin:** Writing - review & editing. **Pan Feng:** Resources. **H.J.H. Brouwers:** Supervision, Writing - review & editing. **Qingliang Yu:** Supervision, Writing - review & editing.

Declaration of Competing Interest

The authors declare that they have no known competing financial interests or personal relationships that could have appeared to influence the work reported in this paper.

Acknowledgements

The authors appreciate the financial supports from the National Natural Science Foundation of China (No. 1706222, No. 51708108), the China Scholarship Council (No. 201806090146), and Eindhoven University of Technology (TU/e). The authors gratefully acknowledge M.Sc. Bin Meng (Building Performance group of TU/e) for his help in processing self-cleaning performance characterization data, and Prof. Albert Schenning and M.Sc. Xinglong Pan (Stimuli-responsive Functional Materials & Devices group of TU/e) for their support and suggestions in the spectrum analysis discussion.

References

[1] P. Berdahl, H. Akbari, L.S. Rose, Aging of reflective roofs: soot deposition, Appl. Opt. 41 (2002) 2355, https://doi.org/10.1364/AO.41.002355.
[2] M. Sleiman, T.W. Kirchstetter, P. Berdahl, H.E. Gilbert, S. Quelen, L. Marlot, C.V. Preble, S. Chen, A. Montalbano, O. Rosseler, H. Akbari, R. Levinson, H. Destaillats, Soiling of building envelope surfaces and its effect on solar reflectance - Part II: Development of an accelerated aging method for roofing materials, Sol. Energy Mater. Sol. Cells. 122 (2014) 271–281, https://doi.org/10.1016/j.solmat.2013.11.028.
[3] M.Z. Guo, T.C. Ling, C.S. Poon, Photocatalytic NOx degradation of concrete surface layers intermixed and spray-coated with nano-TiO_2: Influence of experimental factors, Cem. Concr. Compos. 83 (2017) 279–289, https://doi.org/10.1016/j.cemconcomp.2017.07.022.
[4] D. Osborn, M. Hassan, S. Asadi, J.R. White, Durability quantification of TiO_2 surface coating on concrete and asphalt pavements, J. Mater. Civ. Eng. 26 (2014) 331–337, https://doi.org/10.1061/(ASCE)MT.1943-5533.0000816.
[5] H. Yu, W. Dai, G. Qian, X. Gong, D. Zhou, X. Li, X. Zhou, The nox degradation performance of nano-TiO_2 coating for asphalt pavement, Nanomaterials. 10 (2020), https://doi.org/10.3390/nano10050897.
[6] S. Lorencik, Q.L. Yu, H.J.H. Brouwers, Design and performance evaluation of the functional coating for air purification under indoor conditions, Appl. Catal. B Environ. 168–169 (2015) 77–86, https://doi.org/10.1016/j.apcatb.2014.12.012.
[7] S. Lorencik, Q.L. Yu, H.J.H. Brouwers, Photocatalytic coating for indoor air purification: Synergetic effect of photocatalyst dosage and silica modification, Chem. Eng. J. 306 (2016) 942–952, https://doi.org/10.1016/j.cej.2016.07.093.
[8] Q.L. Yu, H.J.H. Brouwers, Indoor air purification using heterogeneous photocatalytic oxidation. Part I: Experimental study, Appl. Catal. B Environ. 92 (2009) 454–461, https://doi.org/10.1016/j.apcatb.2009.09.004.
[9] J. Chen, C. sun Poon, Photocatalytic construction and building materials: From fundamentals to applications, Build. Environ. 44 (2009) 1899–1906, https://doi.org/10.1016/j.buildenv.2009.01.002.
[10] E. Boonen, A. Beeldens, Photocatalytic roads: From lab tests to real scale applications, Eur. Transp. Res. Rev. 5 (2013) 79–89, https://doi.org/10.1007/s12544-012-0085-6.
[11] Y. Hendrix, A. Lazaro, Q.L. Yu, H.J.H. Brouwers, Influence of synthesis conditions on the properties of photocatalytic titania-silica composites, J. Photochem. Photobiol. A Chem. 371 (2019) 25–32, https://doi.org/10.1016/j.jphotochem.2018.10.040.
[12] C. Giosuè, Q.L. Yu, M.L. Ruello, F. Tittarelli, H.J.H. Brouwers, Effect of pore structure on the performance of photocatalytic lightweight lime-based finishing mortar, Constr. Build. Mater. 171 (2018) 232–242, https://doi.org/10.1016/j.conbuildmat.2018.03.106.
[13] E. Luévano-Hipólito, A. Martínez-De La Cruz, E. López-Cuellar, Q.L. Yu, H.J.H. Brouwers, Synthesis, characterization and photocatalytic activity of WO_3/TiO_2

for NO removal under UV and visible light irradiation, Mater. Chem. Phys. 148 (2014) 208–213, https://doi.org/10.1016/j.matchemphys.2014.07.034.
[14] D.P. MacWan, P.N. Dave, S. Chaturvedi, A review on nano-TiO_2 sol-gel type syntheses and its applications, J. Mater. Sci. 46 (2011) 3669–3686, https://doi.org/10.1007/s10853-011-5378-y.
[15] J. Yang, S. Mei, J.M.F. Ferreira, Hydrothermal synthesis of TiO_2 nanopowders from tetraalkylammonium hydroxide peptized sols, Mater. Sci. Eng. C. 15 (2001) 183–185, https://doi.org/10.1016/S0928-4931(01)00274-0.
[16] F. Sayilkan, S. Erdemoğlu, M. Asiltürk, M. Akarsu, Ş. Şener, H. Sayilkan, M. Erdemoğlu, E. Arpaç, Photocatalytic performance of pure anatase nanocrystallite TiO_2 synthesized under low temperature hydrothermal conditions, Mater. Res. Bull. 41 (2006) 2276–2285, https://doi.org/10.1016/j.materresbull.2006.04.019.
[17] W. Zhou, Q. Cao, S. Tang, Effects on the size of nano-TiO_2 powders prepared with sol-emulsion-gel method, Powder Technol. 168 (2006) 32–36, https://doi.org/10.1016/j.powtec.2006.07.005.
[18] X. Shi, X. Yang, S. Wang, S. Wang, Q. Zhang, Y. Wang, Photocatalytic degradation of rhodamine B dye with high purity anatase nano-TiO_2 synthesized by a hydrothermal method, J. Wuhan Univ. Technol. Mater. Sci. Ed. 26 (2011) 600–605, https://doi.org/10.1007/s11595-011-0275-4.
[19] H. Xu, S. Ouyang, L. Liu, P. Reunchan, N. Umezawa, J. Ye, Recent advances in TiO_2-based photocatalysis, J. Mater. Chem. A. 2 (2014) 12642–12661, https://doi.org/10.1039/c4ta00941j.
[20] R. Vijayalakshmi, V. Rajendran, Synthesis and characterization of nano-TiO_2 via different methods, Arch. Appl. Sci. Res. 4 (2012) 1183–1190, https://doi.org/10.11648/j.nano.20140201.11.
[21] P. Alphonse, A. Varghese, C. Tendero, Stable hydrosols for TiO_2 coatings, J. Sol-Gel Sci. Technol. 56 (2010) 250–263, https://doi.org/10.1007/s10971-010-2301-y.
[22] J.X. Yu, R.A. Chi, J. Guo, Desorption and photodegradation of methylene blue from modified sugarcane bagasse surface by acid TiO_2 hydrosol, Appl. Surf. Sci. 258 (2012) 4085–4090, https://doi.org/10.1016/j.apsusc.2011.12.106.
[23] D. Reyes-Coronado, G. Rodríguez-Gattorno, M.E. Espinosa-Pesqueira, C. Cab, R. De Coss, G. Oskam, Phase-pure TiO_2 nanoparticles: Anatase, brookite and rutile, Nanotechnology. 19 (2008), https://doi.org/10.1088/0957-4484/19/14/145605.
[24] B.K. Mutuma, G.N. Shao, W.D. Kim, H.T. Kim, Sol-gel synthesis of mesoporous anatase-brookite and anatase-brookite-rutile TiO_2 nanoparticles and their photocatalytic properties, J. Colloid Interface Sci. 442 (2015) 1–7, https://doi.org/10.1016/j.jcis.2014.11.060.
[25] T.X. Liu, Y. Liu, Z.J. Zhang, F.B. Li, X.Z. Li, Comparison of aqueous photoreactions with TiO_2 in its hydrosol solution and powdery suspension for light utilization, Ind. Eng. Chem. Res. 50 (2011) 7841–7848, https://doi.org/10.1021/ie102584j.
[26] O.B. Pavlova-Verevkina, S.N. Chvalun, E.D. Politova, V.V. Nazarov, L.A. Ozerina, A.N. Ozerin, Study of the stable nanocrystalline TiO_2 hydrosol and its fractions, J. Sol-Gel Sci. Technol. 35 (2005) 91–97, https://doi.org/10.1007/s10971-005-1311-7.
[27] E. Burunkaya, M. Akarsu, H. Erdem Çamurlu, Ö. Kesmez, Z. Yeşil, M. Asiltürk, E. Arpaç, Production of stable hydrosols of crystalline TiO_2 nanoparticles synthesized at relatively low temperatures in diverse media, Appl. Surf. Sci. 265 (2013) 317–323, https://doi.org/10.1016/j.apsusc.2012.11.003.
[28] X. Ding, S. Pan, C. Lu, H. Guan, X. Yu, Y. Tong, Hydrophobic photocatalytic composite coatings based on nano-TiO_2 hydrosol and aminopropyl terminated polydimethylsiloxane prepared by a facile approach, Mater. Lett. 228 (2018) 5–8, https://doi.org/10.1016/j.matlet.2018.05.103.
[29] E. Ghenne, F. Dumont, C. Buess-Herman, Stability of TiO_2 hydrosols synthesized by hydrolysis of titanium tetraethoxide, Coll. Surf. A Physicochem. Eng. Asp. 131 (1998) 63–67.
[30] M.M. Soderzhinova, D.V. Tarasova, F.K. Chibirova, Aging of titania hydrosols prepared via ultrasonic processing, Inorg. Mater. 52 (2016) 470–475, https://doi.org/10.1134/S0020168516050162.
[31] Y. Wang, Y. He, Q. Lai, M. Fan, Review of the progress in preparing nano TiO_2: An important environmental engineering material, J. Environ. Sci. (China) 26 (2014) 2139–2177, https://doi.org/10.1016/j.jes.2014.09.023.
[32] M. Malekshahi Byranvand, A.N. Kharat, L. Fatholahi, Z. Malekshahi Beiranvand, A review on synthesis of nano-TiO_2 via different methods, J. Nanostructures. 3 (2013) 1–9.
[33] S. Singh, T. Shi, R. Duffin, C. Albrecht, D. van Berlo, D. Höhr, B. Fubini, G. Martra, I. Fenoglio, P.J.A. Borm, R.P.F. Schins, Endocytosis, oxidative stress and IL-8 expression in human lung epithelial cells upon treatment with fine and ultrafine TiO_2: Role of the specific surface area and of surface methylation of the particles, Toxicol. Appl. Pharmacol. 222 (2007) 141–151, https://doi.org/10.1016/j.taap.2007.05.001.
[34] X. Jiang, M. Manawan, T. Feng, R. Qian, T. Zhao, G. Zhou, F. Kong, Q. Wang, S. Dai, J.H. Pan, Anatase and rutile in evonik aeroxide P25: Heterojunctioned or individual nanoparticles?, Catal. Today. 300 (2018) 12–17, https://doi.org/10.1016/j.cattod.2017.06.010.
[35] L. Yang, A. Hakki, F. Wang, D.E. Macphee, Photocatalyst efficiencies in concrete technology: The effect of photocatalyst placement, Appl. Catal. B Environ. 222 (2018) 200–208, https://doi.org/10.1016/j.apcatb.2017.10.013.
[36] C. Nickel, J. Angelstorf, R. Bienert, C. Burkart, S. Gabsch, S. Giebner, A. Haase, B. Hellack, H. Hollert, K. Hund-Rinke, D. Jungmann, H. Kaminski, A. Luch, H.M. Maes, A. Nogowski, M. Oetken, A. Schaeffer, A. Schiwy, K. Schlich, M. Stintz, F. Von Der Kammer, T.A.J. Kuhlbusch, Dynamic light-scattering measurement comparability of nanomaterial suspensions, J. Nanoparticle Res. 16 (2014), https://doi.org/10.1007/s11051-014-2260-2.
[37] Z. Wang, Q. Yu, F. Gauvin, P. Feng, R. Qianping, H.J.H. Brouwers, Nanodispersed TiO_2 hydrosol modified Portland cement paste: The underlying role of hydration on self-cleaning mechanisms, Cem. Concr. Res. 136 (2020), https://doi.org/10.1016/j.cemconres.2020.106156 106156.
[38] M.V. Diamanti, R. Paolini, M. Rossini, A.B. Aslan, M. Zinzi, T. Poli, M.P. Pedeferri, Long term self-cleaning and photocatalytic performance of anatase added mortars exposed to the urban environment, Constr. Build. Mater. 96 (2015) 270–278, https://doi.org/10.1016/j.conbuildmat.2015.08.028.
[39] M.V. Diamanti, B. Del Curto, M. Ormellese, M.P. Pedeferri, Photocatalytic and self-cleaning activity of colored mortars containing TiO_2, Constr. Build. Mater. 46 (2013) 167–174, https://doi.org/10.1016/j.conbuildmat.2013.04.038.
[40] E. Jimenez-Relinque, J.R. Rodriguez-Garcia, A. Castillo, M. Castellote, Characteristics and efficiency of photocatalytic cementitious materials: Type of binder, roughness and microstructure, Cem. Concr. Res. 71 (2015) 124–131, https://doi.org/10.1016/j.cemconres.2015.02.003.
[41] Q.L. Yu, Y. Hendrix, S. Lorencik, H.J.H. Brouwers, Field study of NO_x degradation by a mineral-based air purifying paint, Build. Environ. 142 (2018) 70–82, https://doi.org/10.1016/j.buildenv.2018.06.014.
[42] O.B. Pavlova-Verevkina, N.V. Kul'kova, E.D. Politova, Y.A. Shevchuk, V.V. Nazarov, Preparation of thermostable highly dispersed titanium dioxide from stable hydrosols, Colloid J. Russ. Acad. Sci. Kolloidn. Zhurnal. 65 (2003) 226–229, https://doi.org/10.1023/A:1023329527799.
[43] A.S. Almusallam, Y.M. Abdulraheem, M. Shahat, P. Korah, Aggregation behavior of Titanium Dioxide nanoparticles in aqueous environments, J. Dispers. Sci. Technol. 33 (2012) 728–738, https://doi.org/10.1080/01932691.2011.567886.
[44] N. Veronovski, P. Andreozzi, C. La Mesa, M. Sfiligoj-Smole, V. Ribitsch, Use of Gemini surfactants to stabilize TiO_2 P25 colloidal dispersions, Colloid Polym. Sci. 288 (2010) 387–394, https://doi.org/10.1007/s00396-009-2133-x.
[45] C. Jacobs, R.H. Müller, Production and characterization of a budesonide nanosuspension for pulmonary administration, Pharm. Res. 19 (2002) 189–194, https://doi.org/10.1023/A:1014276917363.
[46] S. Bhattacharjee, DLS and zeta potential - What they are and what they are not?, J. Control. Release. 235 (2016) 337–351, https://doi.org/10.1016/j.jconrel.2016.06.017.
[47] Y. Agrawal, V. Patel, Nanosuspension: An approach to enhance solubility of drugs, J. Adv. Pharm. Technol. Res. 2 (2011) 81, https://doi.org/10.4103/2231-4040.82950.
[48] U. Nobbmann, M. Connah, B. Fish, P. Varley, C. Gee, S. Mulot, J. Chen, L. Zhou, Y. Lu, F. Sheng, J. Yi, S.E. Harding, Dynamic light scattering as a relative tool for assessing the molecular integrity and stability of monoclonal antibodies, Biotechnol. Genet. Eng. Rev. 24 (2007) 117–128, https://doi.org/10.1080/02648725.2007.10648095.
[49] K.S.W. Sing, D.H. Everet, R.A.W. Haul, L. Moscou, R.A. Pierotti, J. Rouquerol, T. Siemieniewska, Reporting physisorption data for gas/solid systems with special reference to the determination of surface area and porosity, Pure Appl. Chem. 57 (1985) 603–619.
[50] A.R. Liu, S.M. Wang, Y.R. Zhao, Z. Zheng, Low-temperature preparation of nanocrystalline TiO_2 photocatalyst with a very large specific surface area, Mater. Chem. Phys. 99 (2006) 131–134, https://doi.org/10.1016/j.matchemphys.2005.10.003.
[51] K.P. Kumar, J. Kumar, K. Keizer, Effect of Peptization on Densification and Phase-Transformation Behavior of Sol–Gel-Derived Nanostructured Titania, J. Am. Ceram. Soc. 77 (1994) 1396–1400, https://doi.org/10.1111/j.1151-2916.1994.tb05426.x.
[52] A.P. Werle, M.L. De Souza, K. Loh, R. Ando, V.M. John, The performance of a self-cleaning cool cementitious surface, Energy Build. 114 (2016) 200–205, https://doi.org/10.1016/j.enbuild.2015.06.025.